Title
Microzooplankton regulation of surface ocean POC:PON ratios

Journal
Global Biogeochemical Cycles, 30(2)

ISSN
0886-6236

Authors
Talmy, D
Martiny, AC
Hill, C
et al.

Publication Date
2016-02-01

DOI
10.1002/2015gb005273

Peer reviewed

AGU PUBLICATIONS

Global Biogeochemical Cycles

RESEARCH ARTICLE
10.1002/2015GB005273

Key Points:
- Mean surface ocean particulate organic carbon:nitrogen ratios (POC:PON) are relatively homeostatic
- Under nitrogen limitation, phytoplankton have elevated carbon-to-nitrogen (C:N) ratios
- Interactions between primary and secondary producers control average POC:PON of surface particulates

Correspondence to:
D. Talmy,
dtalmy@mit.edu

Citation:
Talmy, D., A. C. Martiny, C. Hill, A. E. Hickman, and M. J. Follows (2016), Microzooplankton regulation of surface ocean POC:PON ratios, *Global Biogeochem. Cycles*, *30*, 311–332, doi:10.1002/2015GB005273.

Received 25 AUG 2015
Accepted 11 JAN 2016
Accepted article online 13 JAN 2016
Published online 23 FEB 2016

Microzooplankton regulation of surface ocean POC:PON ratios

D. Talmy[1], A. C. Martiny[2], C. Hill[1], A. E. Hickman[3], and M. J. Follows[1]

[1]Department of Earth, Atmosphere and Planetary Sciences, Massachusetts Institute of Technology, Cambridge, Massachusetts, USA, [2]Departments of Earth System Science and Ecology and Evolutionary Biology, University of California, Irvine, California, USA, [3]Ocean and Earth Science, University of Southampton, National Oceanography Centre, Southampton, Southampton, UK

Abstract The elemental composition of particulate organic matter in the surface ocean significantly affects the efficiency of the ocean's store of carbon. Though the elemental composition of primary producers is an important factor, recent observations from the western North Atlantic Ocean revealed that carbon-to-nitrogen ratios (C:N) of phytoplankton were significantly higher than the relatively homeostatic ratio of the total particulate pool (particulate organic carbon:particulate organic nitrogen; POC:PON). Here we use an idealized ecosystem model to show how interactions between primary and secondary producers maintain the mean composition of surface particulates and the difference between primary producers and bulk material. Idealized physiological models of phytoplankton and microzooplankton, constrained by laboratory data, reveal contrasting autotrophic and heterotrophic responses to nitrogen limitation: under nitrogen limitation, phytoplankton accumulate carbon in carbohydrates and lipids while microzooplankton deplete internal C reserves to fuel respiration. Global ecosystem simulations yield hypothetical global distributions of phytoplankton and microzooplankton C:N ratio predicting elevated phytoplankton C:N ratios in the high-light, low-nutrient regions of the ocean despite a lower, homeostatic POC:PON ratio due to respiration of excess carbon in systems subject to top-down control. The model qualitatively captures and provides a simple interpretation for, a global compilation of surface ocean POC:PON data.

1. Introduction

The elemental composition of particulate matter in the surface ocean has significant implications for the role of the ocean in mediating atmospheric CO_2. The productivity of the ocean is typically regulated by the availability of macronutrients and micronutrients [*Moore et al.*, 2013] and not inorganic carbon. Thus, the ratio in which carbon is associated with N, P, and Fe (and other potentially limiting elemental resources) in sinking organic particles or subducted dissolved organic matter critically controls the efficiency of the ocean's biological carbon pump [*Volk and Hoffert*, 1985]. *Redfield* [1934] first characterized the composition of particulate organic matter in the ocean, revealing a relatively constant C:N:P of approximately 106:16:1 in surface particulate material. Based, in part, on early data compilations by *Fleming* [1940], the chemical composition of particulate organic matter in the ocean is frequently interpreted to reflect that of the resident autotrophic population [*Goldman et al.*, 1979; *Engel et al.*, 2002; *Martiny et al.*, 2013a], and this canonical ratio has typically been adopted to represent the relative flow of these elements in ocean carbon cycle models [e.g., *Gnanadesikan et al.*, 2002; *Watson and Orr*, 2003]. However, when photosynthetic capacity exceeds the energetic and carbon demands for synthesis of N- and P-rich macromolecules (proteins, nucleic acids, and some lipids), the C:N and C:P ratio of phytoplankton greatly exceeds the canonical Redfield ratio [*Geider and La Roche*, 2002; *Laws and Bannister*, 1980; *Ågren*, 2004]. For example, *Goldman et al.* [1979] report C:N of nitrogen-limited *Dunaliella tertiolecta* as high as 20:1 and C:P of phosphorus-limited *Monochrysis lutheri* as high as 1300:1.

Large areas of the oceans have the conditions to imbalance photosynthetic and nutrient assimilation capacity. In samples from the nutrient-depleted, western North Atlantic Ocean, *Martiny et al.* [2013b] recorded C:N ratios of *Prochlorococcus*, *Synechococcus*, and small eukaryotes all in excess of the Redfield ratio. However, these high ratios were not reflected in the ratio of the coincident bulk particulate matter (Figure 1). Consistent with the high C:N of primary producers observed by *Martiny et al.* [2013b], several studies have independently documented carbon overconsumption (i.e., the consumption of inorganic carbon and nitrogen in ratios exceeding Redfield), both by measuring directly the C:N incorporation ratio via ^{14}C and ^{15}N isotope experiments

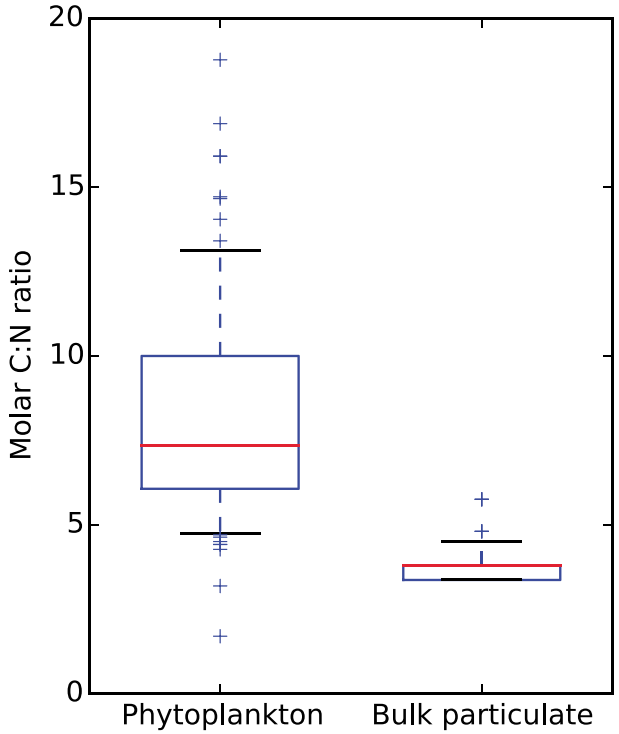

Figure 1. The C:N of phytoplankton is significantly higher than that of bulk particulate matter in samples recorded in warm, nutrient-depleted waters of the western North Atlantic Ocean (64.17°W, 31.67°N) [*Martiny et al.*, 2013b]. Each box represents 73 measurements taken within the top 100 m of the water column. Phytoplankton samples were sorted using flow cytometry and composed mainly of *Prochlorococcus*, *Synechococcus*, and small eukaryotes. In total, the three groups composed 38 ± 21% of particulate organic carbon and 42 ± 25% of particulate organic nitrogen. Individually, *Prochlorococcus*, *Synechococcus*, and small eukaryotes had mean ratios of 10.1 ± 0.5%, 9.1 ± 0.3%, and 8.7 ± 0.3 (±SE), respectively, and the ratios of all three groups were above the bulk value [*Martiny et al.*, 2013b]. The red lines show the median of each sample, blue boxes are first and third quartiles, whereas the lower and upper whiskers show the 5 and 95% confidence intervals, respectively. Blue crosses are outliers.

[*Le Bouteiller*, 1993] and by inferring C:N uptake from changes in dissolved inorganic carbon and nitrogen concentration [*Sambrotto et al.*, 1993; *Körtzinger et al.*, 2001; *Martz et al.*, 2014]. Despite apparent overconsumption, the vast majority of measurements suggest C:N of particulate organic matter (POC:PON) typically fall within a relatively low range (4–10) [*Le Bouteiller*, 1993; *Schneider et al.*, 2003; *Hickman et al.*, 2012; *Martiny et al.*, 2013b] and do not reflect the full range of observations for autotrophic consumption and biomass. Two connected questions arise: What causes phytoplankton uptake and biomass stoichiometry to differ from that of the overall particulate organic matter? What causes the observed overconsumption of carbon?

Here we argue that taking an ecosystem view and considering the role of secondary producers can reconcile these observations. It has been shown that while autotrophs limited by nutrient supply accumulate carbon reserves [*Rodolfi et al.*, 2009; *Griffiths and Harrison*, 2009], microzooplankton under the same restriction deplete them [*Meunier et al.*, 2012]. Using mathematical models, we demonstrate that during the transfer of biomass from primary producers to higher trophic levels, the energy costs of assimilation reduce excess carbon and regulate ecosystem elemental composition, which differs from that of the primary producers. We develop models of primary and secondary producer elemental composition and implement them in a three-dimensional ocean circulation model (MITgcm) [*Marshall et al.*, 1997]. The coupled model is highly idealized, resolving just sufficient detail to address the questions raised. It qualitatively captures pertinent aspects of the elemental composition of the ecosystem and its observed regional variations. It provides a hypothesis for the reconciliation of differences between phytoplankton and total particulate C:N ratios and carbon overconsumption.

In the following sections, we compare predictions of phytoplankton and microzooplankton stoichiometry with laboratory observations. We describe the ecosystem model and its coupling with MITgcm and present simulations of phytoplankton and microzooplankton C:N ratio over the entire surface ocean.

Table 1. Biological Source and Sink Equations for Phytoplankton and Microzooplankton[a]

Phytoplankton Physiological Equations

$$S_{C^i_{R,p}} = \underbrace{\left(P^i_n - \left(\frac{1}{\eta_F} + \zeta_p\right)\mu^i_p - r^i_{C,p}\right)\cdot N^i_{F,p}}_{\text{photosynthesis-biosynthesis-respiration}} - \underbrace{\frac{C^i_{R,p}}{C^i_{R,p}+C^i_{F,p}} G^i_n N^i_{F,z}}_{\text{grazing}} - \underbrace{m^i_p C^i_{R,p}}_{\text{other mortality}} \quad (25)$$

$$S_{N^i_{R,p}} = \underbrace{\left(V^i_n - \mu^i_p\right)\cdot N^i_{F,p}}_{\text{nutrient uptake-biosynthesis}} - \underbrace{\frac{N^i_{R,p}}{N^i_{R,p}+N^i_{F,p}} G^i_n N^i_{F,z}}_{\text{grazing}} - \underbrace{m^i_p N^i_{R,p}}_{\text{other mortality}} \quad (26)$$

$$S_{N^i_{F,p}} = \underbrace{\mu^i_p \cdot N^i_{F,p}}_{\text{biosynthesis}} - \underbrace{\frac{N^i_{F,p}}{N^i_{R,p}+N^i_{F,p}} G^i_n N^i_{F,z}}_{\text{grazing}} - \underbrace{m^i_p N^i_{F,p}}_{\text{other mortality}} \quad (27)$$

Zooplankton Physiological Equations

$$S_{C_{R,z}} = \underbrace{\left(\lambda_z \frac{1}{\eta_p}\sum_i G^i_n - \left(\frac{1}{\eta_F} + \zeta_z\right)\mu_z - r_{C,z}\right)\cdot N_{F,z}}_{\text{grazing-biosynthesis-respiration}} - \underbrace{m_z C_{R,z}}_{\text{other mortality}} \quad (28)$$

$$S_{N_{R,z}} = \underbrace{\left(\lambda_z \sum_i G^i_n - \mu_z - r_{N,z}\right)\cdot N_{F,z}}_{\text{grazing-biosynthesis-respiration}} - \underbrace{m_z N_{R,z}}_{\text{other mortality}} \quad (29)$$

$$S_{N_{F,z}} = \underbrace{\mu_z \cdot N_{F,z}}_{\text{biosynthesis}} - \underbrace{m_z N_{F,z}}_{\text{other mortality}} \quad (30)$$

Particulate Detrital Matter Equations

$$S_{\text{PDC}} = \underbrace{\sum_i \beta^{\text{mort},i}_p m_p \left(C^i_{R,p} + \frac{1}{\eta_F} N^i_{F,p}\right)}_{\text{phytoplankton mortality}} + \underbrace{\beta^{\text{mort}}_z m_z \left(C^i_{R,z} + \frac{1}{\eta_F} N^i_{F,z}\right)}_{\text{microzooplankton mortality}} + \underbrace{\frac{1}{\eta_p}\left(\sum_i G^i_n N^i_{F,z}\right)\beta^{\text{graz}}_p (1-\lambda_z)}_{\text{sloppy feeding}} - \underbrace{r_{\text{PDC,remin}}\text{PDC}}_{\text{remineralization}} \quad (31)$$

$$S_{\text{PDN}} = \underbrace{\sum_i \beta^{\text{mort},i}_p m_p \left(N^i_{R,p} + N^i_{F,p}\right)}_{\text{phytoplankton mortality}} + \underbrace{\beta^{\text{mort}}_z m_z \left(N^i_{R,z} + N^i_{F,z}\right)}_{\text{microzooplankton mortality}} + \underbrace{\left(\sum_i G^i_n N^i_{F,p}\right)\beta^{\text{graz}}_p (1-\lambda_z)}_{\text{sloppy feeding}} - \underbrace{r_{\text{PDN,remin}}\text{PDN}}_{\text{remineralization}} \quad (32)$$

[a]Each equation corresponds to a specific model compartment in Figure 2. All "*i*" superscripts denote parameters and variables that are phytoplankton cell size specific. For clarity, only the summary equations are provided here; the full definitions of each process are provided in Table A2.

We compare the C:N of modeled phytoplankton, microzooplankton, and detritus with a published compilation of overall POC:PON ratio [*Martiny et al.*, 2013b] and, finally, consider the implications for large-scale biogeochemistry.

2. Models and Methods

The main ecosystem model parameterization is reported in Table 1. In the sections that follow, we explain and justify the full equations used to parameterize phytoplankton and microzooplankton physiology. We then describe model implementation in a global ocean ecosystem context and compare simulations with a published compilation of relevant ocean data.

2.1. Physiological Models

We developed physiological models that resolve the main C- and N-containing subcellular components in photo-autotrophs and heterotrophic grazers (Figure 2 and Table 1). We account for the significance of size constraints on autotrophic growth by resolving two size classes since size dependence may have a significant effect on regional variations of photo-autotrophic C:N in the ocean [*Talmy et al.*, 2014]. For both physiological models we briefly outline the details and constraint by published laboratory culture data. Full variable and parameter definitions can be found in Appendix A and Tables A1 and A2.

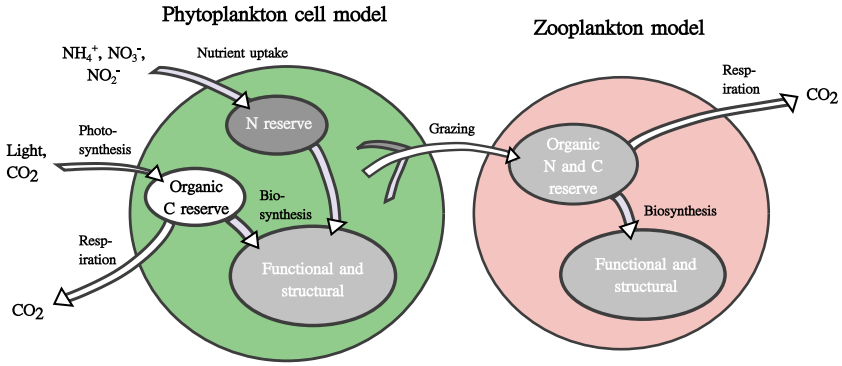

Figure 2. Schematic of modeled elemental flow for representative phytoplankton and microzooplankton types. The full Nutrient-Phytoplankton-Zooplankton-Detritus (NPZD) model actually has two phytoplankton size classes that are not shown here because the physiological model is representative for both groups. For both groups, phytoplankton accumulate intracellular stores of nitrogen and carbon via nutrient uptake and photosynthesis. Internal stores are then synthesized into proteins and associated structural membranes, at an energy cost parameterized as respiration [*Geider and Osborne*, 1989]. Phytoplankton cellular material is then consumed by grazers. Microzooplankton assimilation of food from the reserve compartment into functional cellular apparatus incurs a respiratory cost. Note that, dark grey shapes represent cellular material containing only N, whereas white shapes represent exclusively C-containing compounds. Light grey shapes represent components that contain both N and C. The size of the available carbon reserve for both groups is cell size dependent (Table A2) [*Talmy et al.*, 2014].

2.1.1. Photo-Autotroph Model

Following *Talmy et al.* [2014], the autotroph model is an extension of the internal stores approach [*Droop*, 1983; *Flynn*, 2008] in which three explicit pools are represented (Figure 2) (i) carbon storage as carbohydrates and lipids (Table 1, equation (25)), (ii) nitrogen storage as an inorganic reserve pool (Table 1, equation (26)), and (iii) a functional pool of C and N in the form of proteins and structural membranes with fixed ratio, η_F (see Tables 1 and A1 and equation (27)). The carbon reserve accumulates via photosynthesis, which is assumed to be a saturating function of the ambient irradiance

$$P_n^i = P_m^i \left(1 - \exp\left(-\frac{\alpha^i E}{P_m^i}\right)\right) \tag{1}$$

In equation (1) and all that follow, each *i* superscript denotes parameters and variables that are phytoplankton size class specific. P_n^i is the rate of photosynthesis for phytoplankton size class *i*, P_m^i is the saturation photosynthetic rate, and α^i is the initial slope of the photosynthesis-irradiance curve. The maximum rate of photosynthesis is a linearly decreasing function of the carbon reserve content [*Talmy et al.*, 2014]:

$$P_m^i = \left(1 - \frac{C_{R,p}^i}{C_{R,p}^{\max,i}}\right) P_{\max}^i \gamma_T \tag{2}$$

where $C_{R,p}^i$ is the reserve carbon concentration for size class *i*, $P_{\max}^i$ is the maximum rate of photosynthesis, and γ_T accounts for temperature dependence. The maximum concentration of reserve carbon, $C_{R,p}^{\max,i}$ is expressed as a variable ratio of the total functional nitrogen ($N_{F,p}^i$):

$$C_{R,p}^{\max,i} = \phi_{C,p}^i \frac{1}{\eta_F} N_{F,p}^i \tag{3}$$

where η_F is the stoichiometry of the functional cellular apparatus and $\phi_{C,p}^i$ is a size class-dependent maximal ratio of storage to functional apparatus.

Nutrient uptake rate (V_n^i) is a Michaelis-Menten style function of the ambient substrate concentration:

$$V_n^i = V_m^i \frac{NO_3^-}{NO_3^- + K_S^i} \tag{4}$$

where V_m^i, and K_S^i are the saturation rate and half-saturation constants for nutrient uptake. The saturation value for nutrient uptake is a linearly decreasing function of the reserve nutrient concentration [*Thingstad*, 1987]:

$$V_m^i = \left(1 - \frac{N_{R,p}^i}{N_{R,p}^{\max,i}}\right) V_{\max}^i \gamma_T \tag{5}$$

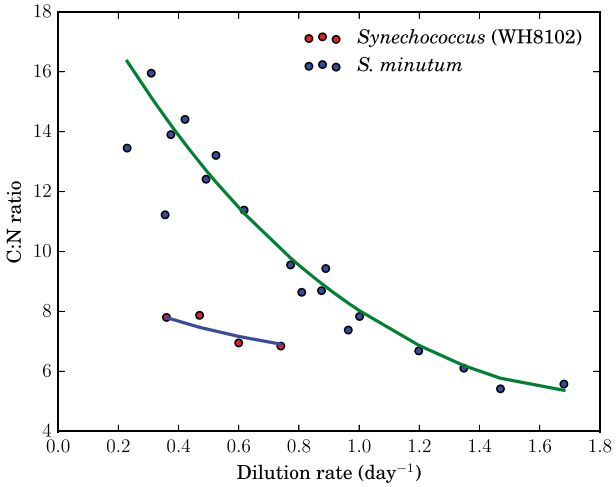

Figure 3. Comparison of the relationship between nitrogen-limited growth rate and cellular C:N ratio between a picoplanktonic and a nanoplanktonic cell. Data for *Synechococcus* WH8102 are from J. Lopez et al. (in review), whereas *S. minutum* data are from *Elrifi and Turpin* [1985]. Solid lines represent manually tuned model fits to the data. In each case, the model was constrained with environmental parameters that matched experimental conditions. *Synechococcus* were grown in NO_3^- limited chemostats on a 14:10 light-dark cycle, 195 µmol photons m^{-2} s^{-1} during the photophase and 24°C throughout. *S. minutum* were also grown in NO_3^--limited chemostats, at a continuous photon flux density of 100 µmol photons m^{-2} s^{-1}, and 20°C. Here *S. minutum* shows extremely flexible C:N ratios in response to resource limitation, whereas *Synechococcus* WH8102 is relatively homeostatic.

where $N^i_{R,p}$ is the reserve nitrogen concentration, $V^i_{\max}$ is the maximal rate of nutrient uptake, and $N^{\max,i}_{R,p}$ is the maximal capacity for internal reserve nitrogen and is expressed as a ratio of the total functional nitrogen

$$N^{\max,i}_{R,p} = \varrho^i_{N,p} N^i_{F,p} \tag{6}$$

where $\varrho^i_{N,p}$ is a maximum ratio of storage to functional N.

The synthesis of proteins and associated structural apparatus depends on Michaelis-Menten functions of the carbon and nitrogen reserves, normalized to the existing concentration of functional apparatus:

$$\mu^i = \min\left\{ \frac{N^i_{R,p}/N^i_{F,p}}{K^i_{N,p} + N^i_{R,p}/N^i_{F,p}}, \frac{C^i_{R,p}/C^i_{F,p}}{K^i_{C,p} + C^i_{R,p}/C^i_{F,p}} \right\} \mu^i_{\max,p} \gamma_T \tag{7}$$

where $K^i_{N,p}$ and $K^i_{C,p}$ are half-saturation constants for nitrogen and carbon limitation and $\mu^i_{\max,p}$ is a size class-specific maximal synthesis rate. At all times, the actual rate of synthesis is taken as the minimum of each separate Michaelis-Menten relation for carbon and nitrogen-limited synthesis [*Talmy et al.*, 2014].

Equations (1) to (7) describing carbon and nitrogen metabolism are coupled in the ecosystem equations presented in Table 1 (Figure 2). Each unit of nitrogen synthesized into functional apparatus incurs a cost of ζ_p carbon units for respiration (Table 1, equation (25)) [*Geider et al.*, 1998]. There is an additional, imposed maintenance respiration cost, $r_{C,p}$, that is independent of growth rate (Table 1, equation (25)). The total cellular carbon-to-nitrogen ratio is calculated by aggregating the functional and reserve carbon and nitrogen concentrations:

$$\eta_p = \frac{N_{R,p} + N_{F,p}}{C_{R,p} + C_{F,p}} \tag{8}$$

Simulations of continuous cultures with both large and small size classes were compared with measurements of cultures grown in chemostats absent of predators. The model was numerically integrated until steady state was reached for a range of dilution rates which matched the experimental conditions. Low dilution rates are expected to lead to nutrient limitation [e.g., *Droop*, 1973]. Nitrogen-limited chemostats with *Synechococcus* WH8102 [*Lopez et al.*, 2016] and *Selenastrum minutum* [*Elrifi and Turpin*, 1985] both show elevated C:N ratios at lower dilution rates, where nitrogen limitation is most intense (red circles, Figure 3) reflecting a reduced capacity to synthesize nitrogen-containing protein and nucleic acids and elevated polysaccharide and/or lipid

synthesis. The range of C:N for the relatively small cyanobacterium is significantly less than the range of C:N for the somewhat larger eukaryote, *S. minutum* (blue circles, Figure 3). By restricting the capacity for carbon storage in the smaller size class, the model captures contrasting responses for small and large phytoplankton cells (solid lines, Figure 3). The cell size dependence of C:N ratio is likely to be an important constraint on regional variations in phytoplankton C:N ratio in the ocean [*Talmy et al.*, 2014].

2.1.2. Microzooplankton Model

The microzooplankton model is conceptually similar and is a simplified version of the previously published model of *Anderson et al.* [2005]. Whereas the model of *Anderson et al.* [2005] was parameterized and tuned for a multicellular heterotroph, we develop and test our model on the microzooplankton *Oxyrrhis marina*. Microzooplankton are the dominant consumers of phytoplankton across the worlds' oceans [*Calbet and Landry*, 2004], and *O. marina* is increasingly used as a model organism to represent this functional group [*Montagnes et al.*, 2011]. The model assumes that the carbon and nitrogen content of ingested prey directly influences the composition of internal reserve material of a typical microzooplankton. Internal C and N reserves may either be assimilated into functional apparatus, or lost due to maintenance and activity respiration. The model accounts separately for unassimilated reserves of N and C (Table 1, equations (28) and (29)), as well as functional and structural apparatus (Table 1, equation (30)). Ingested food contributes directly to the reserve compartments, such that all new additions to the reserves match exactly the C:N concentration of the prey and may thus contain any of the macromolecules (lipids, proteins, etc.), that were present in the food items. We assume that the bulk N in the reserve compartment is homogenous with respect to its effect on growth [cf. *Anderson et al.*, 2004]. The overall rate of ingestion is a saturating function of the prey concentration:

$$G_n^i = \frac{(N_{R,p} + N_{F,p})^2}{(N_{R,p} + N_{F,p})^2 + (K_p^i)^2} G_m^i \tag{9}$$

where K_p^i is a phytoplankton size class-specific half-saturation constant and G_m^i is the saturation value. We impose a Holling type III functional response for predator-prey interactions, reflecting reduced grazing rates when particular prey concentrations are low and alternate food sources are present [*Holling*, 1959, *Gentleman et al.*, 2003]. The maximum rate of ingestion is a decreasing function of the internal reserve nitrogen concentration, which assumes predators with a large internal concentration of unassimilated nitrogen downregulate their rate of consumption:

$$G_m^i = \left(1 - \frac{N_{R,z}}{N_{R,z}^{\max}}\right) G_{\max}^i \gamma_T \tag{10}$$

where $N_{R,z}^{\max}$ and $G_{\max}^i$ are the maximal concentration of microzooplankton reserve N and the maximal grazing rate, respectively. The maximal concentration of reserve nitrogen is again a fixed ratio, $\varrho_{N,z}$ of the functional nitrogen concentration:

$$N_{R,z}^{\max} = \varrho_{N,z} N_{F,p} \tag{11}$$

Assimilation of ingested material depends on the reserve N and C concentration. The rate of assimilation is the minimum of saturating, Michaelis-Menten style functions of carbon and nitrogen reserves, normalized by the existing concentration of functional apparatus:

$$\mu_z = \min\left\{\frac{N_{R,z}/N_{F,z}}{K_{N,z} + N_{R,z}/N_{F,z}}, \frac{C_{R,z}/C_{F,z}}{K_{C,z} + C_{R,z}/C_{F,z}^i}\right\} \mu_{\max,z} \gamma_T \tag{12}$$

where $K_{N,z}$ and $K_{C,z}$ are half-saturation constants for nitrogen and carbon, respectively, and $\mu_{\max,z}$ is a maximal assimilation rate.

Equations (9) to (12) are coupled together in the ecosystem equations in Table 1 (Figure 2), and all parameter units and full definitions are in Table A2. As in the phytoplankton model, assimilation of functional apparatus incurs a respiratory cost, ζ_z (see Table 1, equation (28)), and there is an additional maintenance respiration term that is independent of growth rate ($r_{C,p}$, Table 1, equation (28)). When the microzooplankton reserves have excess C relative to the carbon demand for synthesis of nitrogen reserves into functional material, respiration only draws from the carbon reserve [*Mitra*, 2006]. In the opposing circumstance, respiration incurs a cost from both carbon and nitrogen reserves. Thus, the nitrogen lost due to respiration, $r_{N,z}$, is

$$r_{N,z} = \begin{cases} 0 & \text{if } \eta_z < \eta_F \\ \eta_z(\zeta_z \mu_z + r_{C,z}) & \text{otherwise} \end{cases} \tag{13}$$

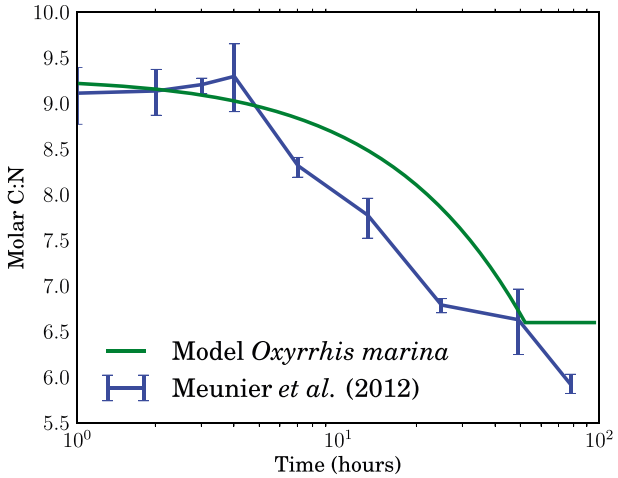

Figure 4. Stoichiometric response of the heterotrophic dinoflagellate *Oxyrrhis marina* to food starvation. The blue lines are experimental results of *Meunier et al.* [2012], whereas the solid green line is derived from the model depicted in Figure 2. In the experiments of *Meunier et al.* [2012], prior to starvation *O. marina* were fed on N-poor *Rhodomonas salina* (C:N = 14.2). At day 1 of the experiment, food supply was cutoff and *O. marina* were left to starve. In the model, the slow decline of C:N over the course of the experiment is attributed to respiration of excess carbon polymers in *Rhodomonas salina*. Thus, heterotrophs limited by food quantity respire excess carbon accumulated by nutrient-poor food supply.

where η_z is the N:C ratio of the microzooplankton population:

$$\eta_z = \frac{N_{R,z} + N_{F,z}}{C_{R,z} + C_{F,z}} \tag{14}$$

Thus, microzooplankton preferentially respire storage carbohydrates and lipids when those compounds are internally available in excess [*Mitra*, 2006]. When grazers run out of storage carbohydrates and lipids, they respire both C and N.

We constrained key parameters of this model by simulating a published laboratory culture experiment (Table A2 and Figure 4). When fed on *Rhodomonas salina* with a C:N ratio of 14.2, the heterotrophic dinoflagellate *Oxyrrhis marina* had a C:N ratio ~9 (beginning of the experiment depicted in Figure 4) [*Meunier et al.*, 2012]. Once the food supply was cut off completely, the C:N ratio of *Oxyrrhis marina* declined over the course of several days (circles, Figure 4) [*Meunier et al.*, 2012]. The microzooplankton model was solved numerically in environmental conditions that matched exactly the experiment of *Meunier et al.* [2012]. The model qualitatively reproduces the time-dependent C:N ratio of *Oxyrrhis marina*, both at the start of the experiment when the heterotroph consumes phytoplankton with a C:N ratio of 14.2 and during the later period of decline (solid line, Figure 4).

In summary, the phytoplankton and microzooplankton models encapsulate contrasting C:N variation in response to nitrogen limitation (Figures A1 and A2): phytoplankton have a reduced capacity to synthesize protein but their ability to fix carbon remains relatively unaffected, leading to high C:N ratios (Figure 3) [*Rodolfi et al.*, 2009, *Griffiths and Harrison*, 2009]. In contrast, when nitrogen limited, microzooplankton respire carbon which is surplus to synthesis requirements, retaining nitrogen and reducing C:N, consistent with the study of *Oxyrrhis marina* [*Meunier et al.*, 2012].

2.2. Global Ocean Ecosystem Model

To explore the ecological implications of these characteristics, we introduce these parameterizations of primary and secondary producer elemental composition into a global ocean ecosystem, biogeochemistry, and circulation model (MITgcm). The ecosystem model simulates flow of C and N between inorganic nutrients, two size classes of photo-autotroph, microzooplankton, and detritus. It is embedded in a coarse-resolution (1° × 1° horizontal, 24 vertical levels), climatologically averaged, global ocean circulation model that has been constrained with satellite and in situ observations [*Wunsch and Heimbach*, 2007]. Since cellular C:N is markedly different in small and large phytoplankton cells, we resolve two size classes: one representative of the cyanobacteria that dominate in the oligotrophic gyres, and another representative of larger eukaryotes, with a relatively large range of C:N values in different growth conditions, following *Talmy et al.* [2014].

Microzooplankton are the dominant consumers of phytoplankton in the worlds oceans [*Calbet and Landry*, 2004], and a single size class consume both small and large cells with equal preference, according to a Holling III-type, saturating function of prey concentration (equation (9)). The flow of material from biomass pools to detritus is treated as in *Ward et al.* [2012], as is remineralization back into inorganic form. For parsimony, the only inorganic pools we resolve explicitly are NO_3^- and dissolved inorganic carbon. The full ecosystem model equations are defined and explained in Appendix A.

2.2.1. Model Parameter Values

In some cases, parameter values were derived using allometry following, e.g., *Ward et al.* [2012] and *Talmy et al.* [2014]. Small and large phytoplankton cells corresponded to populations with average cell diameters of 0.5 and 10 μm, a large enough range to yield contrast between the relatively inflexible C:N of cyanobacteria, and larger eukaryotes [*Talmy et al.*, 2014]. Some parameters were taken from the literature, and those that were not were tuned to the experimental measurements for *Synechococcus*, *S. minutum*, and *O. marina* (Figures 3 and 4). Laboratory experiments do not fully capture real-world environments, and a few parameters that gave suitable fits to the laboratory data, were tuned separately for the ocean model.

2.3. Model-Data Comparisons

The modeled distributions of two phytoplankton size classes, a representative microzooplankton, and the particulate detrital pool are compared with a recently compiled data set of 40,482 observations of the oceanic POC:PON ratio [*Martiny et al.*, 2013a, 2013b]. Particulate organic matter (POM; material collected with filter of pore size ~0.7 μm) may include intact phytoplankton, microzooplankton, detrital material, and particle aggregates. Bulk measurements of the elemental composition of POM reflect contributions of each of these potentially diverse substances. The model presented here resolves spatial and temporal variation in the abundance of phytoplankton and microzooplankton, as well as particulate detritus. To compare simulations and observations, we sampled the model at the time of year and geographic location of each separate observation (i.e., a "point-to-point" comparison [*de Mora et al.*, 2013]). Observed C:N ratios greater than 20 and less than 2 are outside of the ranges reported elsewhere in the literature [*Geider and La Roche*, 2002; *Schneider et al.*, 2003] and were excluded from the analysis. Full details on data collection and analysis can be found in *Martiny et al.* [2013a, 2013b]. We compared the C:N of aggregated phytoplankton, microzooplankton and detrital material with the C:N of bulk particulate material in 12 distinct ocean biomes characterized by contrasting light and nutrient conditions.

3. Results and Discussion: Simulations of Global Surface Ocean C:N Ratios

We present and explore large-scale variations in the biomass and C:N ratios of simulated phytoplankton, microzooplankton, and total particulate material. The simulations are shown to be consistent with in situ observations of POC:PON averaged over 12 distinct ocean regions. The model reveals the significance of secondary producers in modulating the observed elemental composition of the aggregate particulate pool.

3.1. Biomass and Size Structure

The simulated aggregate of phytoplankton and microzooplankton carbon biomass is lowest in the stratified oligotrophic gyres and highest in the eutrophic equatorial upwelling, coastal regions, and higher-latitude seasonally stratified seas (Figure 5a). The basin-scale patterns of phytoplankton biomass are qualitatively consistent with prior studies of phytoplankton biomass distribution [*Moore et al.*, 2004; *Uitz et al.*, 2006; *Gregg and Casey*, 2007; *Westberry et al.*, 2008; *Ward et al.*, 2012]. We did not explicitly resolve the iron cycle and micronutrient limitation, so simulated biomass concentrations in the high-nutrient, low-chlorophyll (HNLC) regions such as the Antarctic [*Hart*, 1934, 1942] and the northeast Pacific subarctic [*McAllister et al.*, 1961] are overestimated.

The partitioning of simulated biomass with size and trophic level (Figure 5b) is plausible and consistent with prior studies: In permanently oligotrophic areas, where phytoplankton grow close to the community minimum resource requirement (i.e., R^*) [*Tilman*, 1982; *Dutkiewicz et al.*, 2009], high surface-area-to-volume ratio is a strong constraint on competitive interactions and picoplankton dominate the autotrophic population. As resource delivery rates increase, predator populations grow in and exert a top-down control on the picoplankton population size, and nutrient limitation no longer prevents large phytoplankton from acquiring resouces. At sufficiently high rates of resource supply, each phytoplankton size class achieves a standing stock of biomass that is determined by top-down influences [*Poulin and Franks*, 2010] (Figure 5b) and resources are passed to the higher trophic level. Thus, in productive systems, larger size classes become more significant in the autotrophic population, consistent with observations [e.g., *Uitz et al.*, 2006; *Brewin et al.*, 2010;

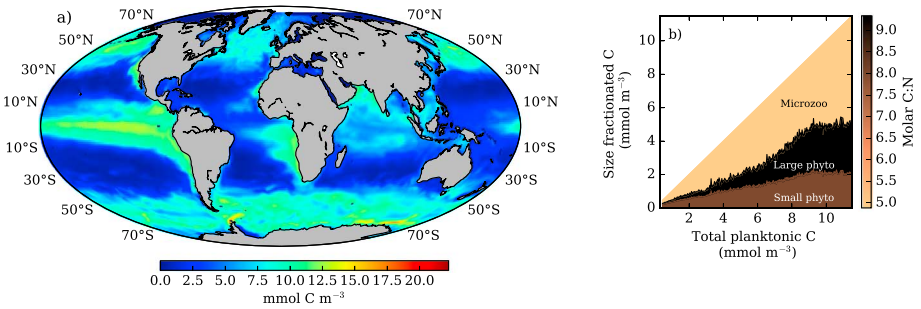

Figure 5. (a) Annually averaged modeled total surface carbon distribution and (b) fractional contributions from each modeled ecosystem member, as a function of total carbon concentration. For both phytoplankton and microzooplankton, the total carbon density is calculated as the sum of each respective carbon reserve compartment, and the carbon content of each "functional and structural" component.

Chisholm, 1992] and richer, size-structured models [*Armstrong*, 1994; *Poulin and Franks*, 2010; *Ward et al.*, 2013]. In addition, in more productive systems, simulated microzooplankton populations constitute an increasingly large proportion of total biomass, also consistent with richer, size-structured models [*Poulin and Franks*, 2010; *Ward et al.*, 2013]. The ratio of modeled microzooplankton to total phytoplankton is on the order 1:1 (g g^{-1}), comparable to measurements of total herbivore to producer ratios in pelagic systems [*Cebrian et al.*, 2009].

3.2. Phytoplankton, Microzooplankton, and Detrital C:N

For both phytoplankton size classes, the model predicts highest phytoplankton C:N in the permanently stratified ocean gyres (Figure 6). Here nutrient limitation is intense, while the photon flux and carbon fixation are enhanced. Large phytoplankton with enhanced storage reach C:N values as high as ~17, whereas small phytoplankton reach maximum ratios of ~10 (Figure 6). In oligotrophic environments, small phytoplankton are superior competitors for nutrients [*Chisholm*, 1992; *Clark et al.*, 2013] and dominate biomass (Figure 5b). Even though large phytoplankton have C:N ratios as high as ~17, the total, aggregated C:N ratio is much lower (Figure 7a), demonstrating significant control of picoplankton on autotrophic elemental composition.

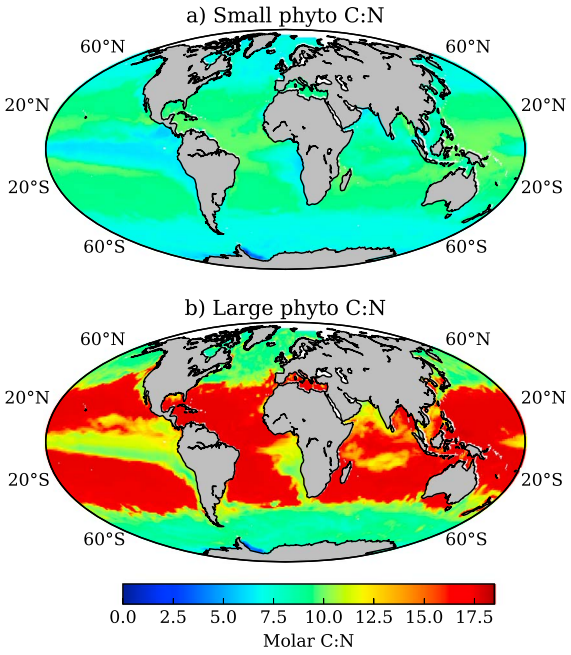

Figure 6. Annually averaged modeled surface C:N ratios for (a) small phytoplankton and (b) large phytoplankton. For these simulations, the model depicted in Figure 2 was coupled with the MITgcm. On average, larger phytoplankton have higher average C:N. For both size classes, nutrient-poor, low-lattitude regions lead to higher C:N ratios than light-limited, high-latitude regions. Equivalent maps for aggregated small and large phytoplankton are depicted in Figure 7.

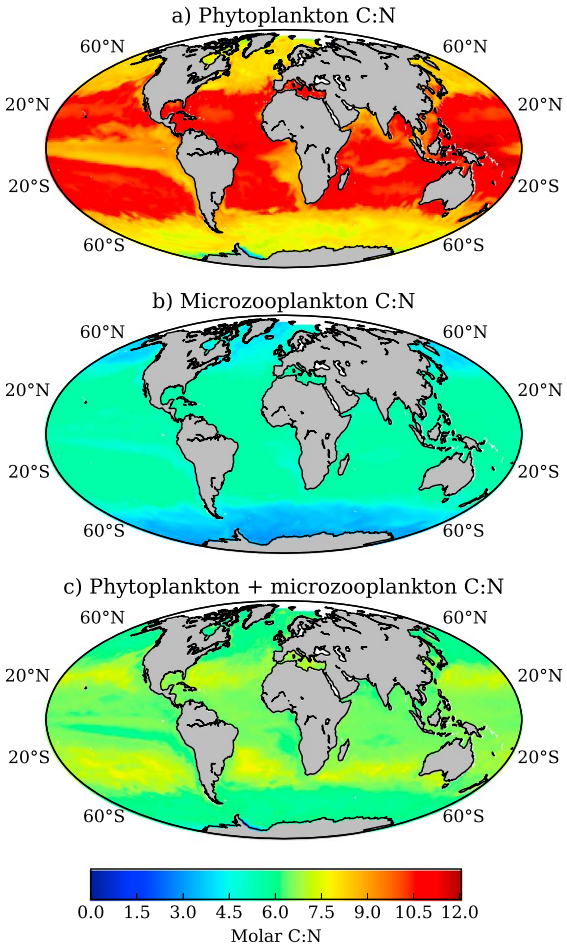

Figure 7. Annually averaged modeled surface C:N ratios for (a) phytoplankton, (b) microzooplankton, and (c) phytoplankton and microzooplankton combined. For these simulations, the model depicted in Figure 2 was coupled with the MITgcm. In all cases, nutrient-poor, low-lattitude regions have higher C:N ratios than light-limited, high-latitude regions. High autotrophic C:N in the gyres is balanced by relatively low, homeostatic microzooplankton C:N in those regions.

In light-stressed, high-latitude ocean environments, nutrients are often available in excess and the C:N ratio of phototrophs is relatively low, for both size classes (Figure 6). In the annual mean, the productive, seasonally stratified surface oceans at high latitude are more light-limited than the oligotrophic gyres, and phytoplankton in those regions do not build such a large reserve of excess carbon (Figure 7a). Similarly, the enhanced nutrient supply in coastal and equatorial upwelling regimes also alleviates nutrient limitation and reduces C:N ratios (Figure 7a).

Similar to the phytoplankton, the highest microzooplankton C:N ratios are in the gyres, with lower values in the coastal upwelling and high-latitude regions (Figure 7b). However, the C:N of modeled microzooplankton in nutrient-limited regions of the ocean is generally significantly lower than that of phytoplankton. The oligotrophic gyres represent a significant challenge to the resident microzooplankton populations; there they are likely to be limited both by food quality and food quantity and a significant proportion of carbon in food is likely to be spent on respiration, driving the C:N of the grazer population down. In more eutrophic subpolar and equatorial regimes, where phytoplankton do not have an excess of carbon, microzooplankton still preferentially respire excess C, but the overall disparity between simulated microzooplankton and phytoplankton elemental composition is lower than in the relatively high-light ocean gyres. The C:N of aggregated phytoplankton and microzooplankton biomass falls in between the two and is typically bracketed by the microzooplankton at its lower limit, and phytoplankton at its upper limit (Figure 7c). Thus, in many parts of the ocean, phytoplankton may only exert a partial influence on the ratio of organic matter, with secondary producers playing an important role.

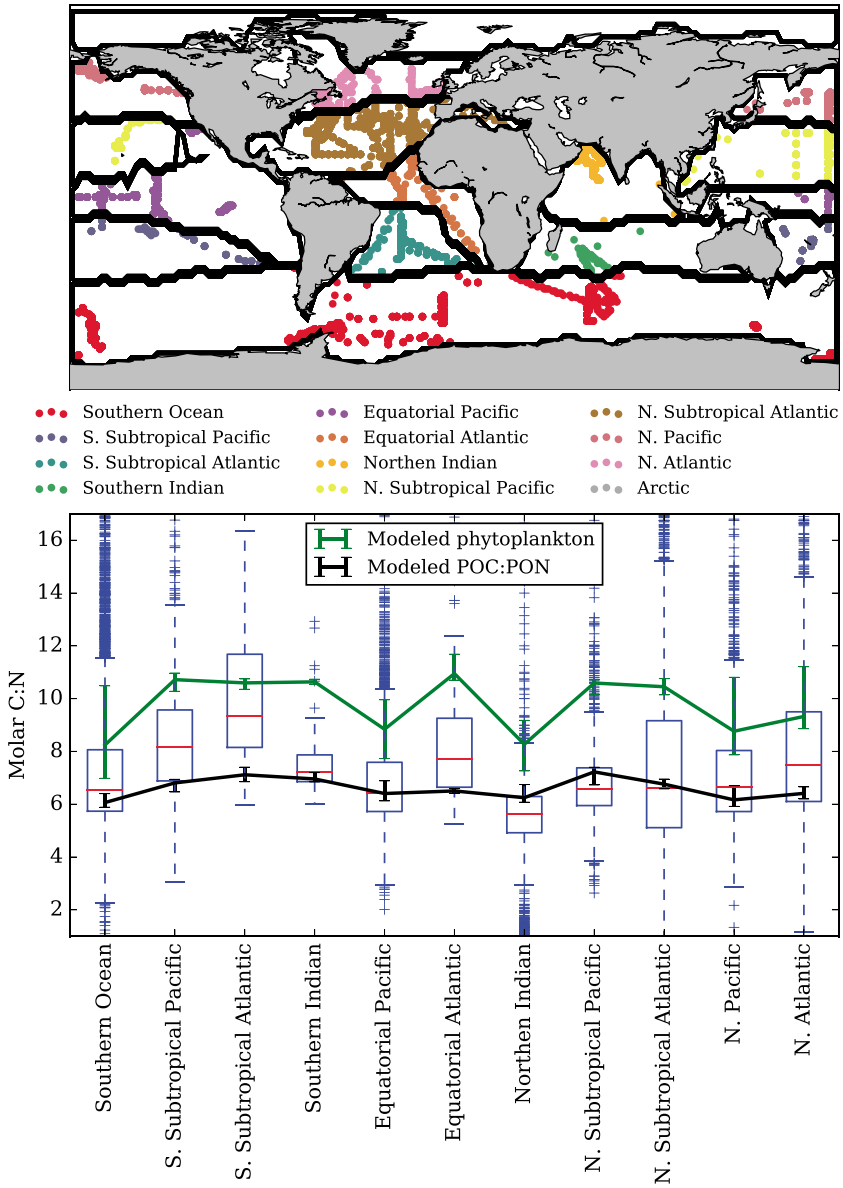

Figure 8. Comparison of model predictions and real-world observations in eleven distinct ocean regimes. (top) Map depicting the boundary of each regime, along with the locations of each sampling station. (bottom) Box and whisker plot comparing the *Martiny et al.* [2013b] compilation of oceanic POC:PON ratios (blue lines and symbols) with the median of combined modeled phytoplankton, microzooplankton, and particulate detrital C:N (black line), along with the C:N of phytoplankton alone (green line). The upper and lower edges of each blue box correspond to the upper and lower quartiles of the data, and the whiskers correspond to the 95% confidence interval. Whiskers on the green and black lines correspond to upper and lower quartiles. When medians are compared, the C:N for aggregated phytoplankton, microzooplankton, and detritus is comparable to the data medians for each ocean domain. In high-light, low-nutrient environments, phytoplankton C:N is consistently higher than Redfield, which is not reflected in the bulk particulates.

To understand the influence of phytoplankton on overall POC:PON ratio, aggregates of modeled phytoplankton, microzooplankton, and particulate detrital biomass were compared with measurements of oceanic POC:PON. The graphs show that the model is consistently within the upper and lower quartiles of POC:PON measurements for the majority of 12 distinct ocean regimes, and well within 95% confidence intervals (Figure 8). Although the model and data have POC:PON ratios close to the canonical Redfield ratio of 6.6, this composition is only partially influenced by the primary producers, whose elemental composition is consistently higher than that of the total particulate, especially in warmer, stratified environments (Figure 7). Cooler waters at high latitude, e.g., the North Atlantic and the Southern Oceans, tend to show closer agreement

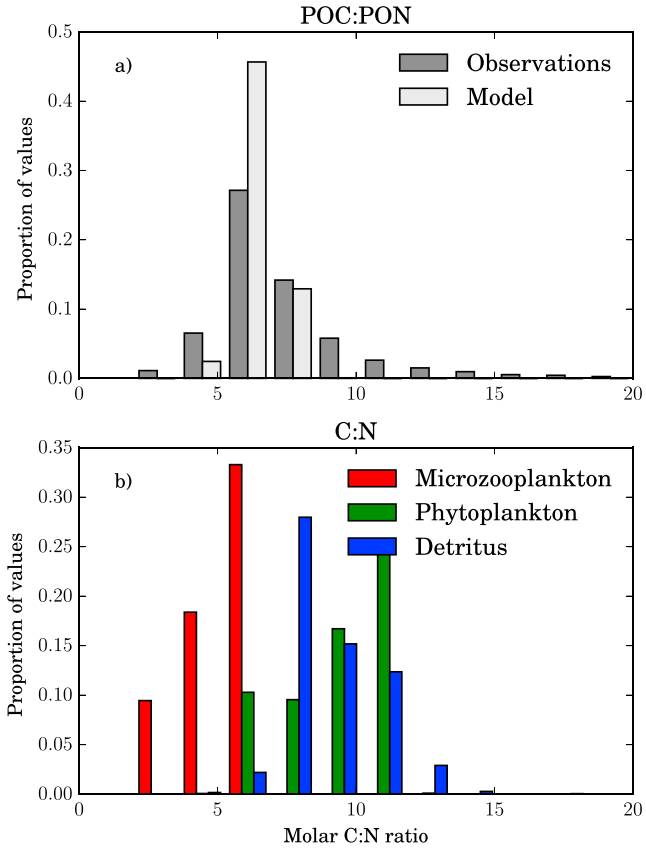

Figure 9. Histograms of stoichiometry comparing (a) observed and modeled carbon-to-nitrogen ratio and (b) modeled phytoplankton, microzooplankton, and detrital carbon-to-nitrogen ratio. The observed carbon-to-nitrogen ratio of POC:PON in Figure 9a is from a compilation by *Martiny et al.* [2013b]. The model result in Figure 9a is C:N ratio for aggregated phytoplankton, microzooplankton, and detritus in the entire ocean domain, derived using the model in Figure 2 coupled to the MITgcm. The median and standard deviations for the modeled C:N ratios in Figure 9a are 6.5 and 0.64, respectively, and the median and standard deviation for the data are 6.6 and 2.5. In general, the model predicts microzooplankton have lower C:N ratio than phytoplankton.

between POC:PON and phytoplankton C:N (Figure 8). Thus, transfer of carbon and nitrogen through trophic levels could be an important control on the overall stoichiometry of organic matter in the ocean, especially in nutrient-stressed, high-light environments such as the oligotrophic gyres.

We compared histograms of the aggregates of phytoplankton, microzooplankton, and detrital biomass with measurements of POC:PON sampled globally, and the results show broad consistency between the model and the data (Figure 9a). We decomposed the C:N of bulk particulate matter into the three main constituents at every observation data point, to reveal systematic differences between the three groups (Figure 9b). Typically, the observed POC:PON ratio is a composite of high-phytoplankton C:N, combined with a microzooplankton population that is somewhat lower. The modeled particulate detritus pool consists of dead phytoplankton and microzooplankton, and a histogram of its C:N ratio represents an amalgam of both groups (Figure 9b). Though appropriate marine observations are not available to test this prediction, it is pleasing that the results are consistent with observations in terrestrial and freshwater ecosystems: there the C:N ratio of autotrophs is generally higher than the C:N of consumers [*Elser et al.*, 2000; *Persson et al.*, 2010].

The C:N ratio of phytoplankton increases systematically, in a linear fashion, as a function of irradiance between the 12 regimes depicted in Figure 8 (Figure 10a). In contrast, the microzooplankton show much less variation as a function of light intensity in each ocean regime (Figure 10a). Measurements of POC:PON also show little variation as a function of average light intensity, which is consistent with the aggregate of modeled phytoplankton, microzooplankton, and detritus (Figures 10b and 10c). Thus, although the ecosystem model suggests the C:N ratio of phototrophs should increase systematically as a function of irradiance, lack of systematic variation in the data is likely due to preferential respiration of carbon by higher trophic levels.

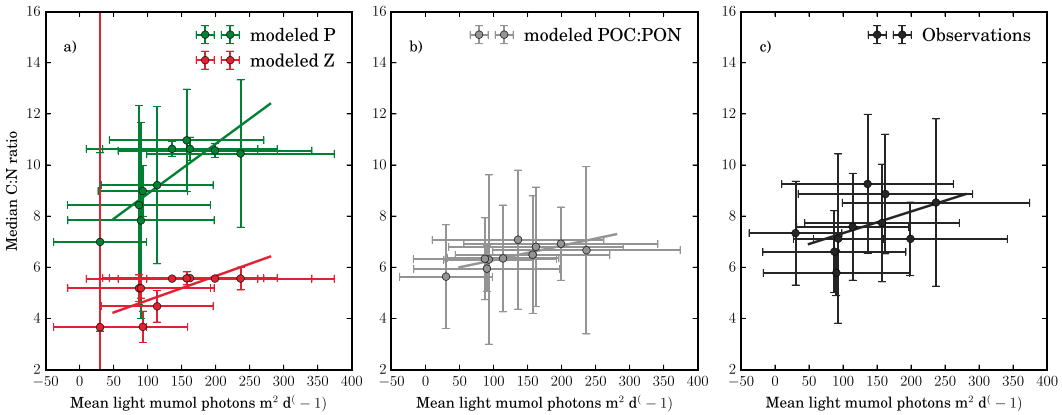

Figure 10. (a) Modeled C:N of phytoplankton (green lines and circles) and microzooplankton (red lines and circles) against average photon flux density (PFD) for the 12 ocean regimes depicted in Figure (8). Also shown is (b) the aggregrate of modeled phytoplankton, microzooplankton, and detrital C:N, along with (c) the observed C:N of particulate organic matter in each regime. Error bars are one standard deviation either side of the mean. Model data used for all averages were obtained by sampling the model at the grid cell corresponding to the time, latitude, and longitude of each sampling station described by *Martiny et al.* [2013b]. Note that the model PFD was used in all calculations. The model predicts a larger discrepancy between phytoplankton and microzooplankton C:N ratio in high-light environments.

3.3. Biogeochemical Implications

The efficiency of the ocean's biological carbon pump depends upon the flux and quality of the material that sinks out of the surface layer [*Broecker*, 1983; *Volk and Hoffert*, 1985], which include detritus originating from phytoplankton and zooplankton in aggregates held together by sticky material [*Fowler and Knauer*, 1986]. The quality of material and the efficiency of the biological pump, depend on the relation between upwelled nutrients assimilated into biomass, and net primary production. The conversion between nutrient assimilation and carbon fixation requires understanding of elemental composition, which is usually assumed to be homogenously Redfield [e.g., *Gnanadesikan et al.*, 2002; *Watson and Orr*, 2003]. If the contributions of phytoplankton- and zooplankton-derived detritus are consistently different, our results (Figures 7–10) could have important implications for our understanding of the biological carbon pump. For example, in the summer time at high latitude, there could be large excess of carbon fixation relative to nutrient uptake, leading to elevated phytoplankton C:N. Elevated phytoplankton C:N may not be evident in measurements of particulate organic matter, but nonetheless constitute a significant portion of material sinking to the deep ocean. Thus, calculations of biological pump efficiency could benefit from understanding of each separate component of the particulate pool in these areas.

3.4. Implications for Ecosystem Health

As well as influencing biological pump efficiency, the phytoplankton C:N ratio can also be used to infer growth rate and ecosystem productivity [*Eppley et al.*, 1973; *Tett et al.*, 1975]. The chemical composition of particulate organic matter in the ocean is frequently interpreted to reflect that of the resident autotrophic population [*Goldman et al.*, 1979; *Engel et al.*, 2002; *Martiny et al.*, 2013a]. Yet recent observations have shown that phytoplankton C:N ratio in nutrient-depleted warm waters of the western North Atlantic Ocean are significantly higher than the C:N ratio of bulk particulate organic matter (Figure 1) [*Martiny et al.*, 2013b, 2013a]. Our results (Figures 8–10), along with previously published meta-analyses of producer and herbivore elemental composition [*Elser et al.*, 2000; *Persson et al.*, 2010], suggest the elemental composition of organic matter is likely to reflect not just the phytoplankton, but aggregated, systematically different constituents. Thus, bulk particulates do not, in general, reflect the elemental composition of phytoplankton and should not be used to infer phytoplankton growth rates. Instead, measurements of individual constituents of particulate organic matter are required.

4. Caveats and Future Needs

This model of oceanic detritus is still highly idealized. We did not account explicitly for bacterial remineralization, which is expected to drive relatively small increases in the C:N ratio of POM at depths well

beneath the euphotic zone due to bacterial preference for nitrogen [*Schneider et al.*, 2003]. Furthermore, we did not account at all for the interplay between the dissolved and particulate pools. Nutrient-stressed phytoplankton are known to excrete carbon-rich transparent exopolymeric polysaccharides (TEP), which contribute to particle aggregation and sinking [*Mari et al.*, 2005; *Schartau et al.*, 2007]. The model assumes all excess carbon is available for remineralization and respiration and does not account for recalcitrant dissolved organic carbon [*Jiao et al.*, 2010] that may enter the POM pool via particle aggregation [*Verdugo et al.*, 2004]. Thus, although the average modeled C:N ratio is consistent with POC:PON observations, the model does not reproduce some high C:N values in the tail of the distribution (Figure 9a). Our physiologically based ecological model is a foundation on which other important processes mentioned here, such as TEP-mediated particle aggregation, may be incorporated in mechanistic biogeochemical models of carbon export.

We modeled just three size classes, a small and large phytoplankton and a microzooplankton grazer. The small phytoplankton was tuned to data for *Synechococcus*, which are extremely abundant in the oligotrophic gyres [*Flombaum et al.*, 2013]. Nonetheless, additional information about C:N variation of other picocyanobacteria and picoeukaryotes would strengthen our predictions of picophytoplankton elemental composition (Figure 6a). The large variation in C:N for the large size class (Figures 3 and 6b) has been observed for a reasonably wide range of larger eukaryotes subjected to nutrient limitation [*Caperon and Meyer*, 1972; *Laws and Wong*, 1978; *Laws and Bannister*, 1980; *Sakshaug et al.*, 1989]. The dinoflagellate *O. marina* is predominately found in coastal environments [*Montagnes et al.*, 2011], and our model would benefit from data describing C:N ratios of microzooplankton that dominate in open ocean environments. Larger, multicellular zooplankton at high lattitude accumulate large lipid stores leading to relatively high C:N ratios [*Forest et al.*, 2011]. If microzooplankton in colder climates adopt a similar metabolic strategy, then C:N ratios at high latitude could be elevated, changing significantly the patterns depicted in Figure 7. Future modeling studies could benefit from incorporating zooplankton metabolic adaptations to high-latitude environments.

The results depicted in Figures 6 to 10 are of course dependent on our choice of parameter values (Table A2). For example, the mean C:N ratio of both phytoplankton and microzooplankton are controlled, to first order, by the assumed composition of functional cellular apparatus (η_F) and changing these values has direct control over the average value of each distribution in (Figure 9b). Furthermore, the capacity for carbon storage in phytoplankton ($\varrho^i_{C,p}$), controls the accumulation of carbon, as do the maintenance respiration costs ($r_{C,p}$, $r_{C,z}$). Enhanced capacity for phytoplankton carbon storage leads to higher overall C:N ratios, whereas enhanced carbon respiration rates deplete carbon reserves and drive down the overall C:N ratio. Parameters controlling small versus large competition for nutrients (e.g., the half saturation for nutrient uptake, K^i_S, equation (4)) influence the contribution of small versus large phytoplankton to total biomass and parameters that control the affinity of microzooplankton for different phytoplankton groups (e.g., the maximum grazing rate ($G^i_{\max}$)) influence the overall ratio of phytoplankton to microzooplankton (Figure 5). Our finding that interactions between small and large phytoplankton and higher trophic levels influence POC:PON ratios points to the need for the most important parameters (e.g., η_F, $\varrho^i_{C,p}$, $r_{C,p}$, $r_{C,z}$, K^i_S, and $G^i_{\max}$) to be well constrained for a range of species occupying different ocean habitats.

Our aim was to encapsulate the basic, underlying mechanisms of autotrophy and heterotrophy by microzooplankton, to assess in isolation their contributions to the chemical composition of particulate organic matter. The data describing bulk POC:PON are insufficient to constrain each of the constituents of particulate organic matter, and our model results (Figures 7–10) should not be treated as precise estimates. We did not explicitly account for the contribution of nitrogen fixation or iron limitation [*Gruber and Sarmiento*, 1997], nor for the cycling and uptake of ammonium [*Dortch*, 1990], or phosphorus, all of which are likely to influence where, when and by how much, nutrient limitation drives an imbalance between photosynthesis and biosynthesis. Phytoplankton limited by iron often do not show large variation in C:N [*Sakshaug and Holm-Hansen*, 1977; *Price*, 2005], and the model may thus overpredict phytoplankton C:N in HNLC regions such as the Antarctic [*Hart*, 1934, 1942] and the northeast Pacific subarctic [*McAllister et al.*, 1961], perhaps due to the high iron requirement of photosynthetic proteins necessary for carbon fixation [*Geider and La Roche*, 1994]. However, our main conclusion that phytoplankton carbon accumulated during nutrient limitation is lost in trophic transfer (Figure 9) does not depend on the precision with which we can reproduce the degree of nutrient limitation in different ocean regimes.

5. Outlook

Understanding the elemental composition of the ocean depends on the underlying metabolic diversity that regulates nutrient storage and assimilation [*Daines et al.*, 2014]. The model presented here resolves the main metabolic processes that regulate metabolism for a small group of representative organisms. Our results point to a need to understand separately the zooplankton, phytoplankton, and detrital contributions to particulate organic matter, for both the biological carbon pump efficiency and diagnosing ecosystem health. Measurements of separate constituents of organic matter have proved challenging in the past, but sorting of phytoplankton from other organic components with flow cytometry [e.g., *Martiny et al.*, 2013b; *Graff et al.*, 2015], is an exciting avenue for more improved understanding of phytoplankton ecophysiology, and ultimately the influence of phytoplankton on carbon cycling in the ocean.

Appendix A: Ecosystem Model Description

Each tracer within the modeled ecosystem is constrained with mass balance equations for advection, mixing, sinking, and biological source and sink terms. In this appendix, we describe the mass balance equations for each significant tracer. The format is very similar to previous descriptions included in, e.g., *Follows et al.* [2007], *Dutkiewicz et al.* [2009, 2012], and *Ward et al.* [2012].

Nitrate mass balance

$$\frac{\partial \mathrm{NO_3^-}}{\partial t} = -\nabla \cdot \left(\mathbf{u}\mathrm{NO_3^-}\right) + \nabla \cdot \left(\mathbf{K}\nabla \mathrm{NO_3^-}\right) + S_{\mathrm{NO_3^-}} \tag{A1}$$

where **u** is a three-dimensional velocity field and **K** is a three-dimensional field of mixing coefficients. The phytoplankton reserve carbon ($C^i_{R,p}$), and all other tracers have exactly the same form and are mentioned here in summary.

$$\frac{\partial C^i_{R,p}}{\partial t} = -\nabla \cdot \left(\mathbf{u}C^i_{R,p}\right) + \nabla \cdot \left(\mathbf{K}\nabla C^i_{R,p}\right) \tag{A2}$$

$$+ S_{C^i_{R,p}} + \frac{\partial \left(w_{p,i}C^i_{R,p}\right)}{\partial z} \tag{A3}$$

Phytoplankton reserve nitrogen ($N^i_{R,p}$) mass balance

$$\frac{\partial N^i_{R,p}}{\partial t} = -\nabla \cdot \left(\mathbf{u}N^i_{R,p}\right) + \nabla \cdot \left(\mathbf{K}\nabla N^i_{R,p}\right) \tag{A4}$$

$$+ S_{N^i_{R,p}} + \frac{\partial \left(w_{p,i}N^i_{R,p}\right)}{\partial z} \tag{A5}$$

Phytoplankton functional apparatus ($N^i_{F,p}$) mass balance

$$\frac{\partial N^i_{F,p}}{\partial t} = -\nabla \cdot \left(\mathbf{u}N^i_{F,p}\right) + \nabla \cdot \left(\mathbf{K}\nabla N^i_{F,p}\right) \tag{A6}$$

$$+ S_{N^i_{F,p}} + \frac{\partial \left(w_{p,i}N^i_{F,p}\right)}{\partial z} \tag{A7}$$

Zooplankton reserve carbon ($C_{R,z}$) mass balance

$$\frac{\partial C_{R,z}}{\partial t} = -\nabla \cdot (\mathbf{u}C_{R,z}) + \nabla \cdot (\mathbf{K}\nabla C_{R,z}) \tag{A8}$$

$$+ S_{C_{R,z}} + \frac{\partial (w_z C_{R,z})}{\partial z} \tag{A9}$$

Zooplankton reserve nitrogen ($N_{R,z}$) mass balance

$$\frac{\partial N_{R,z}}{\partial t} = -\nabla \cdot (\mathbf{u}N_{R,z}) + \nabla \cdot (\mathbf{K}\nabla N_{R,z}) \tag{A10}$$

$$+ S_{N_{R,z}} + \frac{\partial (w_z N_{R,z})}{\partial z} \tag{A11}$$

Table A1. Biological Variables and Non–Size Class-Specific Parameters

Symbol	Description	Value	Units
$C_{R,p}$	Phytoplankton reserve carbon	Variable	mmol C m^{-3}
$C_{F,p}$	Phytoplankton functional carbon	Variable	mmol C m^{-3}
$C_{R,p}^{max}$	Phytoplankton maximum reserve carbon	Variable	mmol C m^{-3}
$N_{R,p}$	Phytoplankton reserve nitrogen	Variable	mmol N m^{-3}
$N_{F,p}$	Phytoplankton functional nitrogen	Variable	mmol N m^{-3}
$N_{R,p}^{max}$	Phytoplankton maximum reserve nitrogen	Variable	mmol N m^{-3}
$C_{R,z}$	Microzooplankton reserve carbon	Variable	mmol C m^{-3}
$C_{F,z}$	Microzooplankton functional carbon	Variable	mmol C m^{-3}
$C_{R,z}^{max}$	Microzooplankton maximum reserve carbon	Variable	mmol C m^{-3}
$N_{R,z}$	Microzooplankton reserve nitrogen	Variable	mmol N m^{-3}
$N_{F,z}$	Microzooplankton functional nitrogen	Variable	mmol N m^{-3}
$N_{R,z}^{max}$	Microzooplankton maximum reserve nitrogen	Variable	mmol N m^{-3}
S	External substrate concentration (nitrate)	Variable	μmol L^{-1}
E	Ambient photon flux density (PFD)	Variable	mol photons m^{-2} d^{-1}
P_n	Carbon fixation rate	Variable	mmol C (mmol N)$^{-1}$ d^{-1}
P_m	Carbon fixation rate at $C_{R,p}$	Variable	mmol C (mmol N)$^{-1}$ d^{-1}
V_n	Nitrogen uptake rate	Variable	day^{-1}
V_m	Maximum nitrogen uptake at $N_{R,p}$	Variable	day^{-1}
G_n	Nitrogen-normalized microzooplankton grazing rate	Variable	mmol C (mmol N)$^{-1}$$d^{-1}$
G_m	Nitrogen-normalized microzooplankton grazing rate at $C_{R,z}$	Variable	mmol C (mmol N)$^{-1}$ d^{-1}
μ_z	Phytoplankton biosynthesis rate	Variable	day^{-1}
μ_p	Microzooplankton biosynthesis rate	Variable	day^{-1}
η_p	N:C phytoplankton	Variable	mmol N (mmol C)$^{-1}$
η_z	N:C microzooplankton	Variable	mmol N (mmol C)$^{-1}$
γ_T	Temperature response	Variable	-
u	Three-dimensional velocity field (u, v, w) from the physical model	Variable	
K	Three-dimensional mixing coefficients from the physical model	Variable	
z	Depth	Variable	m
t	Time	Variable	day
$S_{NO_3^-}$	Biological and other sources and sinks of nitrate	Variable	mmol N m^{-3} d^{-1}
$S^i_{C_{R,p}}$	Biological sources and sinks of reserve phytoplankton carbon	Variable	mmol C m^{-3} d^{-1}
$S^i_{N_{R,p}}$	Biological sources and sinks of reserve phytoplankton nitrogen	Variable	mmol N m^{-3} d^{-1}
$S^i_{N_{F,p}}$	Biological sources and sinks of functional phytoplankton nitrogen	Variable	mmol N m^{-3} d^{-1}
$S_{C_{R,z}}$	Biological sources and sinks of reserve microzooplankton carbon	Variable	mmol C m^{-3} d^{-1}
$S_{N_{R,z}}$	Biological sources and sinks of reserve microzooplankton carbon	Variable	mmol N m^{-3} d^{-1}
$S_{N_{F,z}}$	Biological sources and sinks of functional microzooplankton nitrogen	Variable	mmol N m^{-3} d^{-1}
S_{PDC}	Biological sources and sinks of particulate detrital carbon	Variable	mmol C m^{-3} d^{-1}
S_{PDN}	Biological sources and sinks of particulate detrital nitrogen	Variable	mmol N m^{-3} d^{-1}
S_{DDC}	Biological sources and sinks of dissolved detrital carbon	Variable	mmol C m^{-3} d^{-1}
S_{DDN}	Biological sources and sinks of dissolved detrital nitrogen	Variable	mmol N m^{-3} d^{-1}
$w_{p,i}$	Sinking rate of phytoplankton type i	Variable	m day^{-1}
w_z	Sinking rate of microzooplankton	Variable	m day^{-1}
w_{PDM}	Sinking rate of particulate detrital matter	Variable	m day^{-1}
$r_{PDC,remin}$DDC	Remineralization rate of particulate detrital nitrogen	0.08	day^{-1}
$r_{PDN,remin}$DDN	Remineralization rate of particulate detrital nitrogen	0.08	day^{-1}
$r_{DDC,remin}$DDC	Remineralization rate of particulate detrital nitrogen	0.04	day^{-1}
$r_{DDN,remin}$DDN	Remineralization rate of particulate detrital nitrogen	0.04	day^{-1}

Table A2. Parameter Values for Phytoplankton and Microzooplankton

Parameter	Small Phytoplankton	Large Phytoplankton	Microzooplankton	Units	Description and Source
P^i_{max}	33	47.0	-	mmol C (mmol N)$^{-1}$ d^{-1}	Maximum carbon fixation rate, tuned, Figure 3.
α^i	10.0	10.0	-	m^2 (mol photons)$^{-1}$ mol C (mol N)$^{-1}$	Photosynthesis-irradiance curve initial slope, cell size is thought to influence the initial slope of the photosynthesis-irradiance curve through pigment packaging [*Morel and Bricaud*, 1981], but there is large scatter in allometric relations for light-limited growth [*Edwards et al.*, 2015], so we assume size invariance of light-limited photosynthesis, for the small size range considered here.
V^i_{max}	3.5	8.3	-	day^{-1}	Maximum nutrient uptake rate, allometry [*Litchman et al.*, 2007].
K^i_S	0.09	0.1	-	μmol L^{-1}	Half saturation for nutrient uptake, allometry [*Litchman et al.*, 2007].
G^i_{max}	-	-	8.7	day^{-1}	Maximum grazing rate, allometry [*Ward et al.*, 2012].
K^i_P	1.0	1.0	-	mmol N m^{-3}	Grazing half saturation, allometry [*Ward et al.*, 2012].
$\theta^i_{N,p}$	0.3	1.0	-	-	Maximum ratio of reserve to functional phytoplankton N, tuned, Figure 3.
$\theta^i_{N,z}$	-	-	3.0	-	Maximum ratio of reserve to functional microzooplankton N, tuned, Figure 4.
$\theta^i_{C,p}$	0.6	2.2	-	-	Maximum ratio of reserve to functional phytoplankton C, tuned, Figure 3.
$\theta^i_{C,z}$	-	-	3.0	-	Maximum ratio of reserve to functional microzooplankton C, Figure 4.
$K^i_{C,p}$	0.01	1.0	-	-	Phytoplankton carbon assimilation half saturation, tuned, Figure 3.
$K^i_{N,p}$	0.01	1.0	-	-	Phytoplankton nitrogen assimilation half saturation, tuned, Figure 3.
$K_{C,z}$	-	-	1.0	-	Microzooplankton carbon assimilation half saturation, tuned, Figure 4.
$K_{N,z}$	-	-	1.0	-	Microzooplankton nitrogen assimilation half saturation, tuned, Figure 4.
$\mu_{max,z}$	-	-	1.5	day^{-1}	Microzooplankton maximum assimilation rate, tuned, Figure 4.
$\mu^i_{max,p}$	2.0	4.0	-	day^{-1}	Phytopankton maximum assimilation rate, tuned, Figure 3.
ζ_p	3.0	3.0	-	mmol C (mmol N)$^{-1}$	Phytoplankton cost of biosynthesis [*Pahlow*, 2005].

Table A2. (continued)

Parameter	Small Phytoplankton	Large Phytoplankton	Microzooplankton	Units	Description and Source
ζ_z	-	-	3.0	mmol C (mmol N)$^{-1}$	Microzooplankton cost of biosynthesis, tuned, Figure 4.
η_F	0.15	0.15	0.18	mmol N (mmol C)$^{-1}$	Nitrogen to carbon ratio of functional apparatus. Microzooplankton are more N rich than phytoplankton [see *Persson et al.*, 2010, and references therein].
$r_{C,p}$	-	-	0.01	mmol C (mmol N)$^{-1}$ d^{-1}	Phytoplankton respiration of carbon, tuned.
$r_{N,p}$	-	-	0.01	d^{-1}	Phytoplankton respiration of nitrogen, tuned.
$r_{C,z}$	-	-	0.01	mmol C (mmol N) d^{-1}	Microzooplankton respiration of carbon, tuned.
m_p^i	0.1	0.1	-	day^{-1}	Phytoplankton nongrazing-related mortality, assumed.
m_z	-	-	0.1	day^{-1}	Microzooplankton nongrazing-related mortality, assumed.
$\beta_p^{\mathrm{mort},i}$	0.8	0.5	-	-	Fraction of phytoplankton mortality toward particulate detritus [*Ward et al.*, 2012].
β_z^{mort}	-	-	0.5	-	Fraction of microzooplankton mortality toward particulate detritus [*Ward et al.*, 2012].
β_p^{graz}	0.8	0.5	-	-	Fraction of microzooplankton sloppy feeding toward particulate detritus [*Ward et al.*, 2012].
λ_z	-	-	0.4	-	Microzooplankton assimilation efficiency [*Anderson and Hessen*, 1995].

Zooplankton functional apparatus ($N_{F,z}$) mass balance

$$\frac{\partial N_{F,z}}{\partial t} = -\nabla \cdot (\mathbf{u} N_{F,z}) + \nabla \cdot (\mathbf{K} \nabla N_{F,z}) \tag{A12}$$

$$+ S_{N_{F,z}} + \frac{\partial (w_z N_{F,z})}{\partial z} \tag{A13}$$

Particulate detrital carbon (PDC) mass balance

$$\frac{\partial \mathrm{PDC}}{\partial t} = -\nabla \cdot (\mathbf{u}\mathrm{PDC}) + \nabla \cdot (\mathbf{K} \nabla \mathrm{PDC}) \tag{A14}$$

$$+ S_{\mathrm{PDC}} + \frac{\partial (w_{\mathrm{PDM}} \mathrm{PDC})}{\partial z} \tag{A15}$$

Particulate detrital nitrogen (PDN) mass balance

$$\frac{\partial \mathrm{PDN}}{\partial t} = -\nabla \cdot (\mathbf{u}\mathrm{PDN}) + \nabla \cdot (\mathbf{K} \nabla \mathrm{PDN}) \tag{A16}$$

$$+ S_{\mathrm{PDN}} + \frac{\partial (w_{\mathrm{PDM}} \mathrm{PDN}}{\partial z} \tag{A17}$$

Dissolved detrital carbon (DDC) mass balance

$$\frac{\partial \mathrm{DDC}}{\partial t} = -\nabla \cdot (\mathbf{u}\mathrm{DDC}) + \nabla \cdot (\mathbf{K} \nabla \mathrm{DDC}) + S_{\mathrm{DDC}} \tag{A18}$$

Dissolved detrital nitrogen (DDN) mass balance

$$\frac{\partial \mathrm{DDN}}{\partial t} = -\nabla \cdot (\mathbf{u}\mathrm{DDN}) + \nabla \cdot (\mathbf{K} \nabla \mathrm{DDN}) + S_{\mathrm{DDN}} \tag{A19}$$

Several of the biological source and sink terms are defined in the main text (Table 1). Here we define additional source and sink terms for nitrate, dissolved detrital carbon, and dissolved detrital nitrogen:

$$S_{NO_3^-} = \underbrace{r_{DDN,remin}DDN\gamma_T + r_{DDC,remin}DDC\gamma_T}_{\text{remineralization}} + \underbrace{r_{PDN,remin}PDN\gamma_T + r_{PDC,remin}PDC\gamma_T}_{\text{remineralization}} - \underbrace{\sum_i V_n^i \cdot N_{F,p}^i}_{\text{nutrient uptake}} \tag{A20}$$

$$S_{DDC} = \underbrace{\sum_i \left(1-\beta_p^{mort,i}\right) m_p \left(C_{R,p}^i + \frac{1}{\eta_F} N_{F,p}^i\right)}_{\text{phytoplankton mortality}} + \underbrace{\left(1-\beta_z^{mort}\right) m_z \left(C_{R,z}^i + \frac{1}{\eta_F} N_{F,z}^i\right)}_{\text{microzooplankton mortality}}$$
$$+ \underbrace{\frac{1}{\eta_p}\left(\sum_i G_n^i N_{F,z}^i\right)\right)\left(1-\beta_p^{graz}\right)(1-\lambda_z)}_{\text{sloppy feeding}} - \underbrace{r_{DDC,remin}DDC\gamma_T}_{\text{remineralization}} \tag{A21}$$

$$S_{DDN} = \underbrace{\sum_i \left(1-\beta_p^{mort,i}\right) m_p \left(N_{R,p}^i + N_{F,p}^i\right)}_{\text{phytoplankton mortality}} \tag{A22}$$

$$+ \underbrace{\left(1-\beta_z^{mort}\right) m_z \left(N_{R,z}^i + N_{F,z}^i\right)}_{\text{microzooplankton mortality}}$$
$$+ \underbrace{\left(\sum_i G_n^i N_{F,p}^i\right)\right)\left(1-\beta_p^{graz}\right)(1-\lambda_z)}_{\text{sloppy feeding}}$$
$$- \underbrace{r_{DDN,remin}DDN\gamma_T}_{\text{remineralization}} \tag{A23}$$

The temperature response γ_T follows an Arrenhuis-like equation

$$\gamma_T = e^{R(T-T_{ref})} \tag{A24}$$

where R defines the temperature sensitivity and T_{ref} is a reference temperature at which $\gamma_T = 1$ [*Ward et al.*, 2012] (Table A1).

Acknowledgments
This work is funded in part by the Gordon and Betty Moore Foundation through grant GBMF3778 to M.J. Follows. A.C. Martiny was supported by NSF Dimensions of Biodiversity, grant OCE-1046297. The data in Figure 1 are available as a supplement with *Martiny et al.* [2013a, 2013b]. The data set containing POC:PON observations (Figures 8–10) is available at http://www.bco-dmo.org/dataset/526747. D. Talmy was supported by NSF Biological Oceanography grant OCE-1537951.

References

Ågren, G. (2004), The C:N:P stoichiometry of autotrophs - theory and observations, *Ecol. Lett.*, *7*(3), 185–191, doi:10.1111/j.1461-0248.2004.00567.x.

Anderson, T., and D. Hessen (1995), Carbon or nitrogen limitation in marine copepods?, *J. Plankton Res.*, *17*(2), 317–331, doi:10.1093/plankt/17.2.317.

Anderson, T., M. Boersma, and D. Raubenheimer (2004), Stoichiometry: Linking elements to biochemicals, *Ecology*, *85*(5), 1193–1202, doi:10.1890/02-0252.

Anderson, T., D. Hessen, J. Elser, and J. Urabe (2005), Metabolic stoichiometry and the fate of excess carbon and nutrients in consumers, *Am. Nat.*, *165*(1), 1–15, doi:10.1086/426598.

Armstrong, R. (1994), Grazing limitation and nutrient limitation in marine ecosystems: Steady state solutions of an ecosystem model with multiple food chains, *Limnol. Oceanogr.*, *39*(3), 597–608, doi:10.4319/lo.1994.39.3.0597.

Brewin, R., S. Sathyendranath, T. Hirata, S. Lavender, R. Barciela, and N. Hardman-Mountford (2010), A three-component model of phytoplankton size class for the Atlantic Ocean, *Ecol. Modell.*, *221*(11), 1472–1483, doi:10.1016/j.ecolmodel.2010.02.014.

Broecker, W. (1983), Ocean chemistry during glacial time, *Geochim. Cosmochim. Acta*, *46*(8), 1539–1540, doi:10.1016/0016-7037(83)90315-0.

Calbet, A., and M. Landry (2004), Phytoplankton growth, microzooplankton grazing, and carbon cycling in marine systems, *Limnol. Oceanogr.*, *49*(1), 51–57, doi:10.4319/lo.2004.49.1.0051.

Caperon, J., and J. Meyer (1972), Nitrogen-limited growth of marine phytoplankton—I. Changes in population characteristics with steady-state growth rate, *Deep Sea Res.*, *19*(387), 601–618.

Cebrian, J., J. Shurin, E. Borer, B. Cardinale, J. Ngai, M. Smith, and W. Fagan (2009), Producer nutritional quality controls ecosystem trophic structure, *PLoS One*, *4*(3), e4929, doi:10.1371/journal.pone.0004929.

Chisholm, S. (1992), Phytoplankton size, in *Primary Productivity and Biogeochemical Cycles in the Sea*, pp. 213–237, Springer, New York.
Clark, J., T. Lenton, H. Williams, and S. Daines (2013), Environmental selection and resource allocation determine spatial patterns in picophytoplankton cell size, *Limnol. Oceanogr.*, *58*(3), 1008–1022, doi:10.4319/lo.2013.58.3.1008.
Daines, S., J. Clark, and T. Lenton (2014), Multiple environmental controls on phytoplankton growth strategies determine adaptive responses of the N:P ratio, *Ecol. Lett.*, *17*(4), 414–425, doi:10.1111/ele.12239.
de Mora, L., M. Butenschön, and J. Allen (2013), How should sparse in situ measurements be compared to continuous model data?, *Geosci. Model Dev. Discuss.*, *5*, 2311–2345, doi:10.5194/gmdd-5-2311-2012.
Dortch, Q. (1990), The interaction between ammonium and nitrate uptake in phytoplankton, *Mar. Ecol. Prog. Ser.*, *61*, 183–201, doi:10.3354/meps061183.
Droop, M. (1973), Some thoughts on nutrient limitation in algae, *J. Phycol.*, *9*, 264–272.
Droop, M. (1983), 25 years of algal growth kinetics, *Bot. Mar.*, *26*, 99–112.
Dutkiewicz, S., M. Follows, and J. G. Bragg (2009), Modeling the coupling of ocean ecology and biogeochemistry, *Global Biogeochem. Cycles*, *23*, GB4017, doi:10.1029/2008GB003405.
Dutkiewicz, S., B. Ward, F. Monteiro, and M. Follows (2012), Interconnection of nitrogen fixers and iron in the Pacific Ocean: Theory and numerical simulations, *Global Biogeochem. Cycles*, *26*, GB1012, doi:10.1029/2011GB004039.
Edwards, K., M. Thomas, C. Klausmeier, and E. Litchman (2015), Light and growth in marine phytoplankton: Allometric, taxonomic, and environmental variation, *Limnol. Oceanogr.*, *60*, 540–552, doi:10.1002/lno.10033.
Elrifi, I., and D. Turpin (1985), Steady state luxury consumption and the concept of optimum nutrient ratios: A study with phosphate and nitrate limited selenatrum (chlorophyta), *J. Phycol.*, *21*, 592–602.
Elser, J., et al. (2000), Nutritional constraints in terrestrial and freshwater food webs, *Nature*, *408*, 578–580, doi:10.1038/35046058.
Engel, A., S. Goldthwait, U. Passow, and A. Alldredge (2002), Temporal decoupling of carbon and nitrogen dynamics in a mesocosm diatom bloom, *Limnol. Oceanogr.*, *47*(3), 753–761, doi:10.4319/lo.2002.47.3.0753.
Eppley, R., E. Renger, E. Venrick, and M. Mullin (1973), A study of plankton dynamics and nutrient cycling in the central gyre of the North Pacific Ocean, *Limnol. Oceanogr.*, *18*(4), 534–551, doi:10.4319/lo.1973.18.4.0534.
Flombaum, P., et al. (2013), Present and future global distributions of the marine Cyanobacteria Prochlorococcus and Synechococcusx, *Proc. Natl. Acad. Sci. U.S.A.*, *110*, 9824–9829, doi:10.1073/pnas.1307701110.
Fleming, R. (1940), Composition of plankton and units for reporting populations and production, *Oceanogr. Mar. Biol.*, *3*, 535–540.
Flynn, K. (2008), Use, abuse, misconceptions and insights from quota models—The droop cell quota model 40 years on, *Oceanogr. Mar. Biol. Annu. Rev.*, *46*, 1–23.
Follows, M., S. Dutkiewicz, S. Grant, and S. Chisholm (2007), Emergent biogeography of microbial communities in a model ocean, *Science*, *315*, 1843–1846, doi:10.1126/science.1138544.
Forest, A., V. Galindo, G. Darnis, S. Pineault, C. Lalande, J. Tremblay, and L. Fortier (2011), Carbon biomass, elemental ratios (C:N) and stable isotopic composition (δ13C, δ15N) of dominant calanoid copepods during the winter-to-summer transition in the Amundsen Gulf (Arctic Ocean), *J. Plankton Res.*, *33*(1), 161–178, doi:10.1093/plankt/fbq103.
Fowler, S., and G. Knauer (1986), Role of large particles in the transport of elements and organic compounds through the oceanic water column, *Prog. Oceanogr.*, *16*(3), 147–194, doi:10.1016/0079-6611(86)90032-7.
Geider, R., and J. La Roche (2002), Redfield revisited: Variability of C:N:P in marine microalgae and its biochemical basis, *Eur. J. Phycol.*, *37*(1), 1–17, doi:10.1017/S0967026201003456.
Geider, R., and B. Osborne (1989), Respiration and microalgal growth: A review of the quantitative relationship between dark respiration and growth, *New Phytol.*, *112*(3), 327–341, doi:10.1111/j.1469-8137.1989.tb00321.x.
Geider, R., H. MacIntyre, and T. Kana (1998), A dynamic regulatory model of phytoplankton acclimation to light, nutrients and temperature, *Limnol. Oceanogr.*, *43*(4), 679–694.
Geider, R. J., and J. La Roche (1994), The role of iron in phytoplankton photosynthesis, and the potential for iron-limitation of primary productivity in the sea, *Photosynth. Res.*, *39*, 275–301.
Gentleman, W., A. Leising, B. Frost, S. Strom, and J. Murray (2003), Functional responses for zooplankton feeding on multiple resources: A review of assumptions and biological dynamics, *Deep Sea Res., Part II*, *50*(22–26), 2847–2875, doi:10.1016/j.dsr2.2003.07.001.
Gnanadesikan, A., R. Slater, N. Gruber, and J. Sarmiento (2002), Oceanic vertical exchange and new production: A comparison between models and observations, *Deep Sea Res., Part II*, *49*(1–3), 363–401, doi:10.1016/S0967-0645(01)00107-2.
Goldman, J., J. McCarthy, and D. Peavey (1979), Growth rate influence on the chemical composition of phytoplankton in oceanic waters, *Nature*, *279*, 210–215.
Graff, J., T. Westberry, A. Milligan, M. Brown, G. Dall'Olmo, V. Dongen-Vogels, K. Reifel, and M. Behrenfeld (2015), Analytical phytoplankton carbon measurements spanning diverse ecosystems, *Deep Sea Res., Part I*, *102*, 16–25, doi:10.1016/j.dsr.2015.04.006.
Gregg, W., and N. Casey (2007), Modeling coccolithophores in the global oceans, *Deep Sea Res., Part II*, *54*, 447–477, doi:10.1016/j.dsr2.2006.12.007.
Griffiths, M., and S. Harrison (2009), Lipid productivity as a key characteristic for choosing algal species for biodiesel production, *J. Appl. Phycol.*, *21*, 493–507, doi:10.1007/s10811-008-9392-7.
Gruber, N., and J. Sarmiento (1997), Global patterns of marine nitrogen fixation and denitrification, *Global Biogeochem. Cycles*, *11*(2), 235–266, doi:10.1029/97GB00077.
Hart, T. (1934), *On the Phytoplankton of the South-West Atlantic and Bellingshausen Sea, 1929–31: Discovery Reports Vol VIII*, pp. 1–268, Cambridge Univ. Press, Cambridge, England.
Hart, T. (1942), *Phytoplankton Periodicity in Antarctic Surface Waters*, *Discovery Reports Vol XXI*, pp. 263–356, Cambridge Univ. Press, Cambridge, England.
Hickman, A., C. Moore, J. Sharples, M. Lucas, G. Tilstone, V. Krivtsov, and P. Holligan (2012), Primary production and nitrate uptake within the seasonal thermocline of a stratified shelf sea, *Mar. Ecol. Prog. Ser.*, *463*, 39–57, doi:10.3354/meps09836.
Holling, C. (1959), The components of predation as revealed by a study of small-mammal predation of the European Pine Sawfly, *Can. Entomol.*, *91*(5), 293–320, doi:10.4039/Ent91293-5.
Jiao, N., et al. (2010), Microbial production of recalcitrant dissolved organic matter: Long-term carbon storage in the global ocean, *Nat. Rev. Microbiol.*, *8*(8), 593–599, doi:10.1038/nrmicro2386.

Körtzinger, A., W. Koeve, P. Kähler, and L. Mintrop (2001), C:N ratios in the mixed layer during the productive season in the northeast Atlantic Ocean, *Deep Sea Res., Part I*, *48*, 661–688.

Laws, E., and T. Bannister (1980), Nutrient- and light-limited growth of Thalassiosira fluviatilis in continuous culture, with implications for phytoplankton growth in the ocean, *Limnol. Oceanogr.*, *25*(3), 457–473, doi:10.4319/lo.1980.25.3.0457.

Laws, E., and D. Wong (1978), Studies of carbon and nitrogen metabolism by three marine phytoplankton species in nitrate-limited continuous culture, *J. Phycol.*, *7*, 406–417.

Le Bouteiller, A. (1993), Comparison of in-bottle measurements using ^{15}N and ^{14}C, *ICES Mar. Sci. Symp.*, *197*, 121–131.

Litchman, E., C. Klausmeier, O. Schofield, and P. Falkowski (2007), The role of functional traits and trade-offs in structuring phytoplankton communities: Scaling from cellular to ecosystem level, *Ecol. Lett.*, *10*(12), 1170–1181, doi:10.1111/j.1461-0248.2007.01117.x.

Lopez, J. S., N. S. Garcia, D. Talmy, and A. C. Martiny (2016), Diel variability in the elemental composition of the marine cyanobacterium Synechococcus, *J. Plankton Res.*, doi:10.1093/plankt/fbv120.

Mari, X., F. Rassoulzadegan, C. Brussaard, and P. Wassmann (2005), Dynamics of Transparent Exopolymeric Particles (TEP) production by Phaeocystis globosa under N- or P-limitation: A controlling factor of the retention/export balance, *Harmful Algae*, *4*(5), 895–914.

Marshall, J., A. Adcroft, C. Hill, L. Perelman, and C. Heisey (1997), A finite-volume, incompressible Navier Stokes model for studies of the ocean on parallel computers, *J. Geophys. Res.*, *102*(C3), 5753–5766, doi:10.1029/96JC02775.

Martiny, A., C. Pham, F. Primeau, J. Vrugt, J. Moore, S. Levin, and M. Lomas (2013a), Strong latitudinal patterns in the elemental ratios of marine plankton and organic matter, *Nat. Geosci.*, *6*(4), 279–283, doi:10.1038/ngeo1757.

Martiny, A., J. Vrugt, F. Primeau, and M. Lomas (2013b), Regional variation in the particulate organic carbon to nitrogen ratio in the surface ocean, *Global Biogeochem. Cycles*, *27*(3), 723–731, doi:10.1002/gbc.20061.

Martz, T., U. Send, M. Ohman, Y. Takeshita, P. Bresnahan, H. Kim, and S. Nam (2014), Dynamic variability of ocean biogeochemical ratios in the Southern California Current System, *Geophys. Res. Lett.*, *41*, 2496–2501, doi:10.1002/2014GL059332.

McAllister, C., T. Parsons, K. Stephens, and J. Strickland (1961), Measurements of primary production in coastal sea water using a large-volume plastic sphere, *Limnol. Oceanogr.*, *1947*, 237–256.

Meunier, C., J. Haafke, B. Oppermann, M. Boersma, and A. Malzahn (2012), Dynamic stoichiometric response to food quality fluctuations in the heterotrophic dinoflagellate Oxyrrhis marina, *Mar. Biol.*, *159*(10), 2241–2248, doi:10.1007/s00227-012-2009-3.

Mitra, A. (2006), A multi-nutrient model for the description of stoichiometric modulation of predation in micro- and mesozooplankton, *J. Plankton Res.*, *28*(6), 597–611, doi:10.1093/plankt/fbi144.

Montagnes, D. J., et al. (2011), An introduction to the special issue: Oxyrrhis marina, a model organism?, *J. Plankton Res.*, *33*(4), 549–554, doi:10.1093/plankt/fbq121.

Moore, C., et al. (2013), Processes and patterns of oceanic nutrient limitation, *Nat. Geosci.*, *6*(9), 701–710, doi:10.1038/ngeo1765.

Moore, J., S. Doney, and K. Lindsay (2004), Upper ocean ecosystem dynamics and iron cycling in a global three-dimensional model, *Global Biogeochem. Cycles*, *18*, GB4028, doi:10.1029/2004GB002220.

Morel, A., and A. Bricaud (1981), Theoretical results concerning light absorption in a discrete medium, and application to specific absorption of phytoplankton, *Deep Sea Res., Part A*, *28A*(11), 1375–1393.

Pahlow, M. (2005), Linking chlorophyll nutrient dynamics to the Redfield N:C ratio with a model of optimal phytoplankton growth, *Mar. Ecol. Prog. Ser.*, *287*, 33–43.

Persson, J., P. Fink, A. Goto, J. Hood, J. Jonas, and S. Kato (2010), To be or not to be what you eat: Regulation of stoichiometric homeostasis among autotrophs and heterotrophs, *Oikos*, *119*(5), 741–751, doi:10.1111/j.1600-0706.2009.18545.x.

Poulin, F., and P. Franks (2010), Size-structured planktonic ecosystems: Constraints, controls and assembly instructions, *J. Plankton Res.*, *32*(8), 1121–1130, doi:10.1093/plankt/fbp145.

Price, N. (2005), The elemental stoichiometry and composition of an iron-limited diatom, *Limnol. Oceanogr.*, *50*(4), 1159–1171, doi:10.4319/lo.2005.50.4.1159.

Redfield, A. (1934), On the proportions of organic derivatives in sea water and their relation to the composition of plankton, in *James Johnstone Memorial Volume*, pp. 176–192, Univ. Press of Liverpool.

Rodolfi, L., G. Zittelli, N. Bassi, G. Padovani, N. Biondi, G. Bonini, and M. Tredici (2009), Microalgae for oil: Strain selection, induction of lipid synthesis and outdoor mass cultivation in a low-cost photobioreactor, *Biotechnol. Bioeng.*, *102*(1), 100–112, doi:10.1002/bit.22033.

Sakshaug, E., and O. Holm-Hansen (1977), Chemical composition of Skeletonema costatum (Grev.) Cleve And Pavlova (monochrysis) Lutheri (droop) green as a function of nitrate-, phosphate-, and iron-limited growth, *J. Exp. Mar. Bio. Ecol.*, *29*(1), 1–34, doi:10.1016/0022-0981(77)90118-6.

Sakshaug, E., K. Andresen, and D. Kiefer (1989), A steady state description of growth and light absorption in the marine planktonic diatom Skeletonema costatum, *Limnol. Oceanogr.*, *34*(1), 198–205.

Sambrotto, R., G. Savidge, C. Robinson, P. Boyd, T. Takahashi, D. Karl, C. Langdon, D. Chipman, J. Marra, and L. Codispot (1993), Elevated consumption of carbon relative to nitrogen in the surface ocean, *Nature*, *363*, 248–250.

Schartau, M., A. Engel, J. Schröter, S. Thoms, C. Völker, and D. Wolf-Gladrow (2007), Modelling carbon overconsumption and the formation of extracellular particulate organic carbon, *Biogeosciences Discuss.*, *4*, 13–67, doi:10.5194/bgd-4-13-2007.

Schneider, B., R. Schlitzer, G. Fischer, and E. Nothig (2003), Depth-dependent elemental compositions of particulate organic matter (POM) in the ocean, *Global Biogeochem. Cycles*, *17*(2), 1032, doi:10.1029/2002GB001871.

Talmy, D., J. Blackford, N. J. Hardman-Mountford, L. Polimene, M. J. Follows, and R. J. Geider (2014), Flexible C:N ratio enhances metabolism of large phytoplankton when resource supply is intermittent, *Biogeosciences*, *11*(17), 4881–4895, doi:10.5194/bg-11-4881-2014.

Tett, P., J. Cottrell, D. Trew, and B. Wood (1975), Phosphorus quota and the chlorophyll : Carbon ratio in marine phytoplankton, *Limnol. Oceanogr.*, *20*(4), 587–603, doi:10.4319/lo.1975.20.4.0587.

Thingstad, T. (1987), Utilization of N, P, and organic C by heterotrophic bacteria. I. Outline of a chemostat theory with a consistent concept of "maintenance" metabolism, *Mar. Ecol. Prog. Ser.*, *35*, 99–109.

Tilman, D. (1982), *Resource Competition and Community Structure*, Princeton Univ. Press, Princeton, N. J.

Uitz, J., H. Claustre, A. Morel, and S. Hooker (2006), Vertical distribution of phytoplankton communities in open ocean: An assessment based on surface chlorophyll, *J. Geophys. Res.*, *111*, C08005, doi:10.1029/2005JC003207.

Verdugo, P., A. Alldredge, F. Azam, D. Kirchman, U. Passow, and P. Santschi (2004), The oceanic gel phase: A bridge in the DOM-POM continuum, *Mar. Chem.*, *92*, 67–85, doi:10.1029/2002GL016046.

Volk, T., and M. Hoffert (1985), Ocean carbon pumps: Analysis of relative strengths and efficiencies in ocean-drive atmospheric CO_2 changes, *Geophys. Monogr. Ser.*, *32*, 99–110.

Ward, B., S. Dutkiewicz, O. Jahn, and M. Follows (2012), A size-structured food-web model for the global ocean, *Limnol. Oceanogr.*, *57*(6), 1877–1891, doi:10.4319/lo.2012.57.6.1877.

Ward, B., S. Dutkiewicz, and M. Follows (2013), Modelling spatial and temporal patterns in size-structured marine plankton communities: Top-down and bottom-up controls, *J. Plankton Res.*, *36*(1), 31–47, doi:10.1093/plankt/fbt097.

Watson, A., and J. Orr (2003), Carbon dioxide fluxes in the global ocean, in *Ocean Biogeochemistry*, vol. 5, pp. 123–143, Springer, Berlin Heidelberg.

Westberry, T., M. Behrenfeld, D. Siegel, and E. Boss (2008), Carbon-based primary productivity modeling with vertically resolved photoacclimation, *Global Biogeochem. Cycles*, *22*, GB2024, doi:10.1029/2007GB003078.

Wunsch, C., and P. Heimbach (2007), Practical global oceanic state estimation, *Phys. D Nonlinear Phenom.*, *230*(1–2), 197–208, doi:10.1016/j.physd.2006.09.040.